Terrain-aided navigation with an atomic gravimeter

Christian Musso, Bernard Sacleux, Alexandre Bresson, Jean-Michel Allard, Karim Dahia, Yannick Bidel, Nassim Zahzam, Camille Palmier

Terrain-aided navigation with an atomic gravimeter

C. Musso, B. Sacleux, A. Bresson, JM. Allard, K. Dahia, Y. Bidel, N. Zahzam, C. Palmier
ONERA – The French Aerospace Lab

***Abstract*—Cold atom interferometer is a promising technology to obtain a highly sensitive and accurate absolute gravimeter. With the help of an anomalies gravity map, local measurements of gravity allow a terrain-based navigation. This paper follows the one we published in Fusion 2017. Based on an atomic gravimeter we present a method to map the gravity anomaly. We propose a modification of the Laplace-based particle filter so as to make it more robust. Some simulation results demonstrate a better robustness of the proposed filter.**

I. Introduction

This paper follows the one published in Fusion 2017 [1]. The purpose of the paper is to provide a solution for surface or sub-surface navigation by Terrain Matching using an absolute gravimeter. Application of atom interferometry to the inertial navigation sensors has been proposed in [2]. ONERA has developed a compact and robust atom gravimeter, with the support of the French Defense Agency (DGA). Dedicated to measure gravity aboard a boat or a plane, the GIRAFE2 atom gravimeter considered is similar to the one described and used in reference [3].

In section II, we present the improved absolute atom gravimeter GIRAFE2. It is based on the acceleration measurement of a free falling gas of ultra-cold atoms thanks to atom interferometry. In section III, we propose a method for mapping the gravity anomaly. Based on this atomic gravimeter and with the aid of an external sensor delivering the height of the carrier, we develop a method to extract the gravity anomaly. In section IV, we present an improvement of the Laplace-based particle filter for terrain- based navigation [1]. It is based on a multimodal importance function with a heavy tail. Finally, in section V, some simulation results demonstrate, in case of high terrain ambiguities, the robustness of the proposed filter compared with the previous one.

II. Absolute gravimeter based on atom interferometry

The inertial sensor used in numerical simulations provides an absolute measurement of the acceleration (its continuous value and all temporal variations), with the help of a gyro-stabilized platform which maintains an atom accelerometer aligned with the gravity direction despite angular movements of the carrier (Fig. 1).

Fig. 1. Cold atom gravimeter prototype (GIRAFE2), aboard Norlandair Twin-Otter during an airborne gravimetric survey.

The GIRAFE2 atom gravimeter considered is similar to the one described and used in reference [3]. It is based on the acceleration measurement of a free falling gas of ultra-cold atoms thanks to atom interferometry [4], [5]. Precisely, this absolute gravimeter is measuring vertical proper acceleration. It is absolute in the sense that it provides absolute values of acceleration of free-falling rubidium atoms with respect to the baseplate of the instrument.

The test mass is produced from a magneto-optical trap loaded from a background vapor. After the trap loading, a stage of optical molasses and a microwave selection, we obtain a cloud of few millions of atoms at a temperature about few μK. The acceleration of the free falling cloud of ultra-cold atoms is then measured by light pulse atom interferometry (Fig. 2). After this sequence, the interference signal is then obtained by measuring the population of atoms in the two hyperfine states corresponding to the two output ports of the interferometer. This measurement is obtained by a standard fluorescence method. The proportion P of atoms in a specific state can be written as

$$P = P_m - \frac{C}{2}\cos\left(\frac{4\pi T^2}{\lambda}\Gamma\right) \tag{1}$$

where P_m is a constant called offset of the fringe, C is an experimental constant called contrast, λ is the laser wavelength, T the time separation between Raman laser pulses and Γ is the acceleration of the atoms along the direction of the laser beam.
This simple relation (1) is well verified with no drift or

unknown bias at sub mGal level [6] (1mGal $= 10^{-6}g \approx 10^{-5}m/s^2$). This new technology has already been used to build absolute static gravimeter and demonstrates better or equal performances than classical absolute gravimeter. Typical stability demonstrated in this kind of instrument is largely below $100\,\mu$Gal/Hz$^{1/2}$ in static mode. Recent tests have shown the possibility to operate this next generation of inertial sensors on a moving platform such as aircrafts or marine ship [7], [8]. For instance, considering marine ship, due to higher vibration level aboard, absolute measurement at a level of 1mGal / Hz$^{1/2}$ could be awaited under calm sea level.

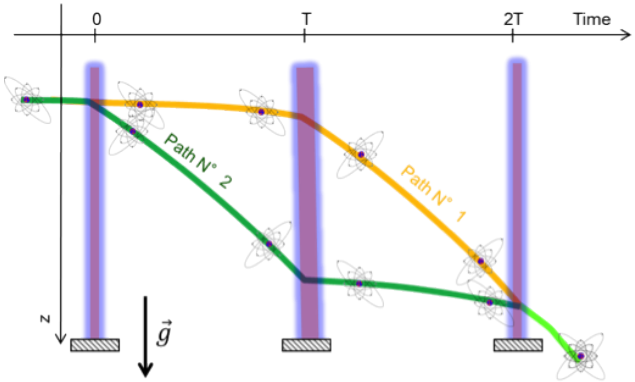

Fig. 2. Spatio-temporal diagram of the atomic free-fall. Output signal is simply proportional to the sinus of the absolute acceleration with a well-defined period.

III. A METHOD TO MAP THE GRAVITY ANOMALY WITH THE ATOMIC GRAVIMETER

The absolute gravimeter described in section II provides local gravity measurements. In the earth-centered, earth-fixed coordinate system (ECEF), the highly nonlinear vertical acceleration model is expressed as follows

$$\Gamma = -g(\phi,\lambda) + \ddot{z} + \underbrace{\gamma_c(\lambda) + \langle 2\,V \times \Omega(\lambda), u_z \rangle}_{\gamma_e \rightarrow \text{Eötvös effect}} \qquad (2)$$

where γ_c is the centripetal acceleration

$$\gamma_c = \frac{V_E^2}{R(\lambda) - z} + \frac{V_N^2}{\frac{R(\lambda)(1-e^2)}{(1-e^2\sin^2(\lambda))} - z} \qquad (3)$$

We assume an ellipsoidal earth modeling. $\langle .,. \rangle$ denotes the inner product and $\times$ the cross product. ϕ is the longitude and λ the latitude. $g(\phi,\lambda)$ is the modulus of the local gravity acceleration vector, $V = [V_N, V_E, V_Z = \dot{z}]^T$ is the carrier speed and u_z is a unit down vertical vector provided by the gyro-stabilized platform (Section II). $\ddot{z}$ is the vertical acceleration due to the carrier movement. $\Omega(\lambda) = \omega\,[\cos(\lambda), 0, -\sin(\lambda)]^T$ is the earth's axis of rotation expressed in the ECEF frame, ω being the earth rotation speed. $R(\lambda)$ is Earth's radius at latitude λ and e is the earth eccentricity.

The local gravity acceleration $g(\phi,\lambda)$ is expressed as the sum of the standard gravity g_0 and the gravity anomaly $g_a(\phi,\lambda)$ (Fig. 3).

$$\begin{cases} g_0(\lambda) = \dfrac{a\,g_e\cos^2(\lambda) + b\,g_p\,\sin^2(\lambda)}{\sqrt{a^2\,\cos^2(\lambda) + b^2\,\sin^2(\lambda)}} \\ g(\phi,\lambda) = g_0(\lambda) + g_a(\phi,\lambda) \end{cases} \qquad (4)$$

where a and b are the equatorial and polar semi-axes, and where g_e, g_p are the gravity accelerations at the equator and poles respectively.

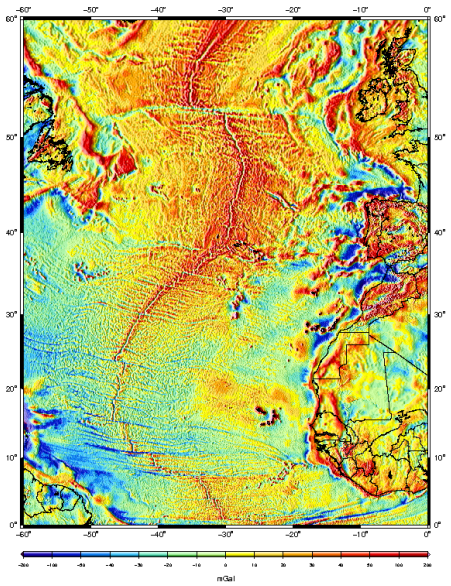

Fig. 3. Gravity anomalies. North atlantic map. Bureau Gravimétrique International (BGI). View of the mid-Atlantic ridge

For the purpose of navigating, developing gravity anomaly maps is required. The use of a carrier instrumentation to obtain coverage over an extended geographical area is a convenient approach in terms of fast mapping. The aim of this section is to propose a method to estimate the gravity anomaly g_a. The difficulty of the experimentation aboard a carrier lies in the spectrum of the acceleration $\ddot{z}(t)$ (2) to which the atomic gravimeter (AG) is subjected. A suitable location of the AG suspension should be not far from the carrier's center of mass. To pick up g_a from the measure $\Gamma(t)$ (2) it is required to estimate $\ddot{z}(t)$ accurately. We propose a method to determine the vertical acceleration $\ddot{z}(t)$ by means of an external measurement of $z(t)$.

A. Mapping the gravity anomaly

The approach described here responds to the scenario where the knowledge of the displacement z according to the local vertical direction is available and accurately known. The vertical acceleration $\ddot{z}(t)$ signal is first determined before extracting g_a from the gravimeter's measure $\Gamma(t)$ (2). We model $z(t)$ as a polynomial of degree $n \geq 2$. We estimate the coefficient $\mathbf{a} = (a_1, ..., a_{n+1})^T$ of this polynomial by means

of the weighted least square method (WLS). Let us introduce the N-vector of the vertical measurements $z_m(t)$ up to time t

$$\mathbf{Z}_m(t) = [z_m(t-(N-1)\Delta t), z_m(t-(N-2)\Delta t), ..., z_m(t)]^T \quad (5)$$

The WLS leads to minimize the following criterion w.r.t $\mathbf{a}$

$$\min_{\mathbf{a}} (\mathbf{Z}_m(t) - H\mathbf{a})^T R (\mathbf{Z}_m(t) - H\mathbf{a}) \quad (6)$$

where the matrix R is a positive semi-definite matrix such that the weights of the measures $z_m(t)$ are greater around the center of $Z_m(t)$ and where

$$\begin{cases} H = [H_{i,j}] \text{ for } i = 1, ..., N \text{ and } j = 1, ..., n+1 \\ H_{i,j} = (i-1)^{j-1}\Delta t^{j-1} \end{cases} \quad (7)$$

The solution of (6) is the following

$$\begin{cases} \hat{\mathbf{a}} = K\ \mathbf{Z_m} \\ K = (H^T R H)^{-1} H^T R \end{cases} \quad (8)$$

The acceleration $\ddot{z}_c$ is estimated at the midpoint $t_c = t - \Delta t_c = t - \frac{(N+1)\Delta t}{2}$ as follows

$$\begin{cases} \hat{\ddot{z}}_c = G\ \hat{\mathbf{a}} \\ G = [G_1, ..., G_{n+1}] \\ \text{with } G_1 = G_2 = 0 \text{ and } G_i = i(i-1)\Delta t_c^{i-2} \text{ for } i \geq 2 \end{cases} \quad (9)$$

Indeed, the acceleration $\hat{\ddot{z}}_c$ is determined by the second derivative of the fitted polynomial with coefficient $\hat{\mathbf{a}}$ at time t_c. The following equation allows us to extract g_a

$$g_a(t) = \ddot{z}_c(t) - g_0(t) - \Gamma(t) - \gamma_e(t) + \nu(t) \quad (10)$$

where $\ddot{z}_c(t)$ is estimated by (9), g_0 is the standard gravity (4), γ_e is the Eötvös effect (2) and where Γ is provided by the atomic gravimeter (2). $\nu(t)$ is a white gaussian noise. The direct extraction of g_a, based on this equation, gives an inaccurate estimation. The signal evolution of the gravity anomaly has a very low frequency w.r.t the error signal affecting $\ddot{z}$. In this context, a low band Kalman filter based on the following 2nd order dynamic is proposed for accurately estimating $g_a(t)$.

$$\ddot{g}_a + 2\,\xi\omega\,\dot{g}_a + \omega^2\,g_a = \eta \quad (11)$$

η is a white gaussian noise, ω is the pulsation depending on the carrier velocity and ξ is a damping coefficient. In order to establish the map (such as Fig. 3), it is necessary to know the position and the velocity of the carrier, the standard gravity g_0 (4), and the Eötvös effect γ_e (2).

B. Simulation results

As an example, a typical $\ddot{z}$ profile during $900s$ of a carrier at a speed of $5m/s$ is illustrated on Fig. 4. The carrier is subjected to an anomaly generated by a second order stochastic process (11) having a pulsation ω close to $5.10^{-5}rd/s$. The power spectral density of the noise η is such that the output of this process gives a 30 mGal s.t.d which is typical for anomaly signal variation (Fig. 5). The discretization of the process is done with a sample frequency $1/\Delta t = 10$ Hz (5). The degree of the polynomial fitting $\ddot{z}$ is $n = 8$. The size of the window (5) is $2\Delta T_c = 10.2s$ ($N = 101$). The s.t.d. of the noises affecting the measurement of $z(t)$ and the gravimeter outputs $\Gamma(t)$ are equal respectively to 0.01m and 1 mGal.

Simulations show that the s.t.d of $\ddot{z}(t) - \hat{\ddot{z}}(t)$ is 383 mGal (Fig. 4). The error of the estimated anomaly obtained by Kalman filtering (11) shows a s.t.d equal to 0.62 mGal (Fig. 6) with a negligible bias. The estimation error of g_a is a colored noise, mainly due to the smoothing method. It is clear that the performance crucially depends on the accuracy of the measurement of $z(t)$.

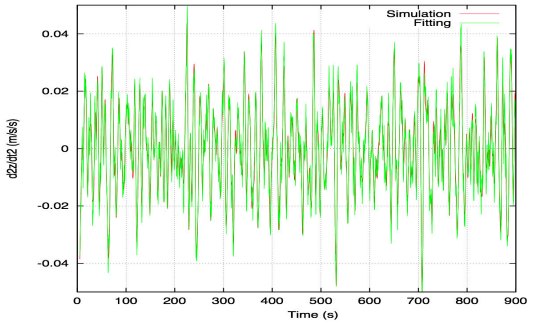

Fig. 4. Time history of $\ddot{z}_t$

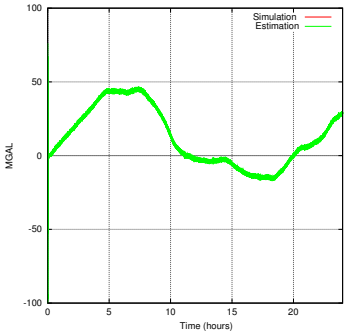

Fig. 5. Typical time history of the gravity anomaly g_a

IV. Gravity anomalies for terrain-aided navigation

The measurement equation is based on the model (2). The carrier is here a boat: the vertical acceleration $\ddot{z}_k$ is considered negligible when the integration time producing the gravity measurement is long enough. The term γ_c will also be ignored as it is negligible in comparison with the anomalies map errors. This leads to the simplified measurement equation

$$Y_k = -g(\phi_k, \lambda_k) + \langle 2\,V \times \Omega(\lambda_k), u_z \rangle + \epsilon_k \quad (12)$$

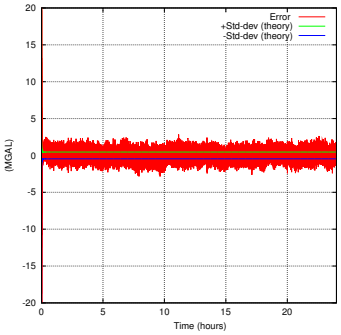

Fig. 6. Time history of the gravity anomaly error after Kalman filtering

where $g(\phi_k, \lambda_k)$ is defined in (4). ϵ_k is a Gaussian with s.t.d σ_g. It is assumed that the carrier follows a constant heading course (rhumb line) with a constant speed at zero altitude. The state is as follows

$$X_k = [\phi_k, \lambda_k, V_N, V_E]^T \tag{13}$$

where ϕ_k and λ_k are the longitude and the latitude at time (k) and where V_N and V_E are the north and east velocities respectively. The vertical velocity is supposed to be null. The dynamics is non-linear and is given by

$$\begin{cases} \lambda_k = \lambda_{k-1} + \dfrac{\Delta T \, \|V\|}{R} \cos(K) \\ \phi_k = \phi_{k-1} + [\varphi(\lambda_k) - \varphi(\lambda_{k-1})] \tan(K) \end{cases} \tag{14}$$

where $\varphi(\lambda) = \log\left[\frac{1+\sin(\lambda)}{\cos(\lambda)}\right]$, where ΔT is the sampling period and K is the heading relative to the north.

In the case of a large uncertainty in the initial state, it is necessary to use a nonlinear filter since the measure (12) is highly nonlinear and multimodal. The particle filter is very convenient and was introduced for the terrain-aided navigation in [9] and was improved later for example in [10]. A large variety of particle filters (PF) has been proposed (see tutorial [11]). We recall the basics of the PF and we propose an improvement of the Multimodal Laplace Particle Filter presented in [1]. This filter has proved to be effective in a multimodal context for the TBD (Track Before Detect) [12], [13], [14].

A. Generic particle filter

Consider the following dynamical and measurement model.

$$\begin{cases} X_k = f_k(X_{k-1}) + \eta_k \\ Y_k = h_k(X_k) + \epsilon_k \end{cases} \tag{15}$$

where f_k and h_k being possibly non-linear functions and where ϵ_k, η_k are zero mean Gaussian noises.
The aim of the PF is to estimate the posterior density

$$p_k(x) \triangleq P(X_k = x | Y_{1:k}) \tag{16}$$

The PF estimates the state given all the measurements until time (k) by means of a Dirac mixture of N weighted particles $\left(X_k^i, w_k^i\right)$

$$p_k(x) \approx \sum_{i=1}^{N} w_k^i \, \delta_{x=X_k^i} \triangleq \hat{p}_k(x) \tag{17}$$

The particles X_k^i evolve according the dynamical model (15) and are corrected through the likelihood

$$\Psi_k(x) \triangleq P(Y_k | X_k = x) \tag{18}$$

The following steps summarize the Sampling Importance Resampling algorithm (SIR) with prior proposal [15]:

1) **Initialisation**: sample $X_0^i \sim p(x_0)$ for $i = 1, \ldots, N$ and set $\omega_0^i = \frac{1}{N}$
2) **Prediction**: sample $X_k^i \sim p\left(X_k = x | X_{k-1}^i\right)$ for $i = 1, \ldots, N$
3) **Measurement update**:
   - compute the weights $\tilde{\omega}_k^i = \omega_{k-1}^i \, \Psi_k(X_k^i)$
   - set $\omega_k^i = \frac{\tilde{\omega}_k^i}{\sum_{j=1}^N \tilde{\omega}_k^j}$
   - compute $\hat{X}_k = \sum_{i=1}^N \omega_k^i X_k^i$
4) **Resampling step**: discard/multiply particles $\left\{X_k^i\right\}$ according to high/low weights ω_k^i

This PF algorithm can be significantly improved when considering importance functions (IF) which take account the current measurement such as the Laplace IF. We recall briefly this algorithm, details are provided in [16], [1].

B. Laplace-based importance function

We ignore for a while the time index (k). Consider an unknown d-dimensional state x distributed according to a prior q and observed through a measurement

$$y = h(x) + \epsilon \tag{19}$$

h being a non-linear function and ϵ a zero mean Gaussian noise. The prior q is not expressed in closed form, only a sample from q is available (it is the case in particle filtering). We suppose in this section that the posterior has a predominant mode. We recall the Laplace method [17] which is useful to design an efficient proposal function. The likelihood $p(y|x)$ is denoted by $\Psi(x)$, the posterior is written as

$$P(X = x | Y = y) \triangleq p(x|y) \propto \Psi(x) \, q(x) \tag{20}$$

We wish to compute an estimate of the posterior. The importance sampling (IS) estimator $\hat{p}$ of $p(x|y)$ is obtained by drawing N samples X^i from a proposal distribution $\tilde{q}$ so that

$$p(x|y) \approx \sum_{i=1}^{N} w^i \, \delta_{x=X^i} \triangleq \hat{p}(x) \tag{21}$$

where $w^i = \frac{\tilde{w}^i}{\sum_{i=1}^N \tilde{w}^i}$ with the following importance weights

$$\tilde{w}^i = \frac{\Psi(X^i) q(X^i)}{\tilde{q}(X^i)} \tag{22}$$

The choice of the proposal distribution is crucial for controlling the Monte Carlo error which can be large if the prior and the likelihood have little overlap (Fig. 7). This is the case for example if the gravity anomalies measurements are very accurate (which is the case with the atom gravimeter). In this case, the information contained in the measurement function is very high and most samples fall in a region where the likelihood is low. It is well-known that the optimal importance function is the posterior $\tilde{q}_{opt}(x) = p(x|y)$. For this purpose, we choose a proposal, for instance a Gaussian, which has moments nearly equal to those of the posterior. The posterior expectation $\mathbb{E}[X|Y]$ and the posterior covariance matrix $\mathbb{V}[X|Y]$ are well approximated by the Laplace formula if the posterior has a predominant mode. The following approximations are in general sufficient [14]

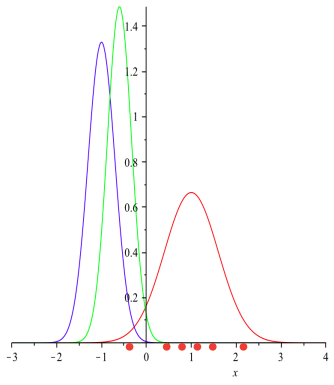

Fig. 7. Small overlap between the prior (red) and the narrow likelihood (blue). Posterior (green)

$$\begin{cases} \mathbb{E}[X|Y] \approx \hat{x} \\ \mathbb{V}[X|Y] \approx \hat{J}^{-1} \end{cases} \tag{23}$$

where $\hat{x}$ is the maximum a posteriori (MAP)

$$\hat{x} = \underset{x \in \mathbb{R}^d}{\arg\max} \{\Psi(x)\, q(x)\} \tag{24}$$

Assuming that the prior $q(x)$ is Gaussian the posterior information matrix J can be approximated by

$$\hat{J} \approx -(\log \Psi)''(\hat{x}) + P^{-1} \tag{25}$$

where P is the covariance matrix of the prior q. The proposal density $\tilde{q}$ is chosen so that it has $\hat{x}$ as mean and $\hat{J}^{-1}$ as covariance matrix

$$\tilde{q} \sim \tilde{q}\,(\hat{x}, \hat{J}^{-1}) \tag{26}$$

Of course, $\tilde{q}$ must be chosen among densities that are easy to sample from. A good criterion for evaluating the accuracy of the approximation (21) is the asymptotic variance of the unnormalized weights $\tilde{w}^i$ [18]

$$\mathbb{V}(\tilde{q}) \approx \frac{1}{N} \left(\frac{\int_{\mathbb{R}^d} \Psi(x)^2 \frac{q(x)^2}{\tilde{q}(x)} dx}{(\int_{\mathbb{R}^d} \Psi(x)\, q(x) dx)^2} - 1 \right) \tag{27}$$

It is suitable for robustness reasons to chose $\tilde{q}$ close to the posterior with heavy tails. Indeed, if, for example, $\tilde{q}$ and q are Gaussian in (27), $q^2/\tilde{q}$ can be unbounded if the s.t.d of $\tilde{q}$ is too small. Therefore, in the sequel, we take $\tilde{q}$ as a multivariate Student distribution.

$$t_d(x; \nu, \mu, \Sigma) = \frac{\Gamma(\frac{\nu+d}{2})(\pi\nu)^{-\frac{\nu}{2}} |\Sigma|^{-1/2}}{\Gamma(\frac{\nu}{2}) \left[1 + (x-\mu)^T \Sigma^{-1} (x-\mu)/\nu\right]^{\frac{\nu+d}{2}}} \tag{28}$$

The smaller the value of ν, the heavier tail is.

C. Approximation of the MAP adapted to the gravity measurement model

In most filtering problems, only a small part of the state vector $X_k = [x_{1,k}, x_{2,k}]^T$ contributes non linearly in the measurement equation:

$$h_k(X_k) = h_k(x_{1,k}, x_{2,k}) = h_1(x_{1,k}) + M(x_{1,k})\, x_{2,k} \tag{29}$$

This is the case in our context where the latitude and the longitude (ϕ_k, λ_k) are the nonlinear contribution in the measurement equation (12). The velocities (V_N, V_E) contribute linearly in the measurement equation. Splitting the state as

$$X_k = [\underbrace{\phi_k, \lambda_k}_{x_{1,k}}, \underbrace{V_N, V_E}_{x_{2,k}}]^T$$

the measurement equation (12) can be expressed as follows:

$$\begin{aligned} Y_k &= -g(\phi_k, \lambda_k) + \langle 2\, V \times \Omega(\lambda_k), u_z \rangle + \epsilon_k \\ &= h_1(x_{1,k}) + M(x_{1,k})\, x_{2,k} + \epsilon_k = h_k(X_k) + \epsilon_k \end{aligned}$$

where

$$M(x_{1,k}) = -2\,\omega\, u_z^T \begin{bmatrix} 0 & \sin(\lambda_k) \\ -\sin(\lambda_k) & 0 \\ 0 & \cos(\lambda_k) \end{bmatrix} \tag{30}$$

We aim to approximate the MAP $\hat{x}_k$ defined as:

$$\hat{x}_k = \underset{x \in \mathbb{R}^4}{\arg\max} \{\Psi_k(x)\, q_k(x)\} \tag{31}$$

where Ψ_k the likelihood (18) and the q_k is the prior (20).

The nonlinear contribution can be handled separately in the maximization (31) under the Gaussian assumption on the prior q_k. This leads to the following algorithm [14] which approximates the MAP.

1) **Minimize** the conditional criterion with respect to x_1

$$\hat{x}_1 = \underset{x_1 \in \mathbb{R}^2}{\arg\min}\ G(x_1)$$

2) **Evaluate** $\hat{x}_2$

$$\hat{x}_2 = \gamma(\hat{x}_1) \tag{32}$$

with $x_1 \in \mathbb{R}^2$ and where $G(x_1)$, described in [1], depends entirely on x_1 and γ is an explicit function of x_1. The prior $q_k(x) = q_k(x_1, x_2)$ is assumed to be Gaussian. The MAP (31) is simply estimated by $\hat{x}_k = [\hat{x}_1, \hat{x}_2]^T$. Finally, the initial 4-dimensional maximization (24) to get the MAP boils down to a 2-dimensional minimization.

D. Improvement of the MM Laplace Particle Filter

In order to address the problem of multimodality due to ambiguities of the gravity anomalies map, we can use a multimodal importance function. At time (k) the posterior has the following form

$$\begin{aligned} p(X_k = x_k|Y_k) &= p(x_{1,k}, x_{2,k}|Y_k) \\ &\propto \Psi_k(x_{1,k}, x_{2,k})\, q_k(x_{1,k}, x_{2,k}) \end{aligned} \tag{33}$$

This posterior can be multimodal, so we need to compute m local MAP $\hat{x}_k^j$ for $j = 1, \cdots, m$ of the posterior (33). This is done in 2 steps as described in (32). We maximize first the 2-dimensional criterion $G(x_{1,k}) = G(\phi_k, \lambda_k)$ over the latitudes and the longitudes to get m local MAP $\hat{x}_{1,k}^j$. The domain of this maximization is restricted to the confidence ellipse (uniform mesh) given by the predicted covariance matrix P_k. P_k is computed empirically with the predicted particles. Then, we compute (32) $\hat{x}_{2,k}^j = \gamma(\hat{x}_{1,k}^j)$ (which corresponds to the north and east velocities) to get the full components of the local MAP $\hat{x}_k^j = (\hat{x}_{1,k}^j, \hat{x}_{2,k}^j)$.
The proposed importance function $\tilde{q}_k^2$ consists in a mixture of m Student distributions (28) centered on the local MAP

$$\begin{cases} \tilde{q}_k^1(x) = \displaystyle\sum_{j=1}^{m} \rho_k^j\, \phi\left(x, \hat{x}_k^j, [\hat{J}_k^j]^{-1}\right) \\ \tilde{q}_k^2(x) = \dfrac{1}{m} \displaystyle\sum_{j=1}^{m} t_d\left(x, \hat{x}_k^j, \Sigma_k\right) \end{cases} \tag{34}$$

where $\Sigma_k = \frac{\nu-2}{\nu} P_k$ such that the covariance of t_d is equal to P_k and where $\tilde{q}_k^1$ is defined in [1] with ϕ being a Gaussian. Laplace-based resampling, i.e generating particles $\tilde{X}_k^i$ according to $\tilde{q}_k^j(x)$ (34), is performed only in case of degeneracy of the weights w_k^i. It replaces the traditional (multinomial) resampling. This degeneracy is detected by the effective sample size of particles $N_{eff} = \frac{1}{\sum_{i=1}^{N} [w_k^i]^2}$ when it is less than a threshold N_{th} [19]. The evaluation of $q_k(\tilde{X}_k^i)$ needed for computing the weights (22) is done by taking the prior equal to a Student distribution (28) centered on the mean of the predicted particles μ_k with $\Sigma_k = \frac{\nu-2}{\nu} P_k$. The algorithm of the proposed PF is described below.

1) **Initialisation** (k=1) For $i = 1, \ldots, N$. Generate the particles $X_{k-1}^i = (x_{1,k-1}^i, x_{2,k-1}^i)$ (positions and velocities) according to the prior. with $w_{k-1}^i \equiv 1/N$

2) **Prediction** For $i = 1, \ldots, N$. Propagate the particles by applying the carrier dynamics (14) $X_{k|k-1}^i = f_k(X_{k-1}^i) + \eta_k^i$

3) **Correction** For $i = 1, \ldots, N$. Compute the likelihood (12) $\Psi_k(X_{k|k-1}^i) = P(Y_k|X_{k|k-1}^i)$ and the weights $w_k^i \propto \Psi_k(X_{k|k-1}^i)\, w_{k-1}^i$ such that $\sum_{i=1}^{N} w_k^i = 1$. Compute $N_{eff} = \frac{1}{\sum_{i=1}^{N} [w_k^i]^2}$
* If $N_{eff} \geq N_{th}$. The corrected particles are $(X_k^i, w_k^i) = (X_{k|k-1}^i, w_k^i)$
* If $N_{eff} < N_{th}$ then perform Laplace-based resampling (34).
- *Compute* the local modes of the posterior (32) : $\hat{x}_k^j = [\hat{x}_{1,k}^j, \hat{x}_{2,k}^j]^T$ for $j = 1, \ldots, m$
- *Generate* samples $\tilde{X}_k^i$ from the proposal $\tilde{q}_k^2$ (34) and compute the importance weights $\tilde{w}_k^i \propto \frac{\Psi_k(\tilde{X}_k^i)\, q_k(\tilde{X}_k^i)}{\tilde{q}_k^2(\tilde{X}_k^i)}$ such that $\sum_{i=1}^{N} \tilde{w}_k^i = 1$ with the prior $q_k \sim t_d(., \mu_k, \Sigma_k)$
The corrected particles are $(X_k^i, w_k^i) = \left(\tilde{X}_k^i, \tilde{w}_k^i\right)$

4) **State estimation** The state is estimated by $\hat{X}_k = \sum_{i=1}^{N} w_k^i\, X_k^i$

Go to the prediction step $k \rightarrow k+1$

V. Simulation Results

We evaluate the performances of the proposed algorithm compared to the original one [1]. For that purpose, we simulate 2 trajectories generating anomaly gravity signals which can be problematic for a particle filter (Fig. 10). The anomaly gravity map (Fig. 8) covers the zone $[-9\,^\circ - 4\,^\circ]$x$[46\,^\circ 49\,^\circ]$ in the longitude-latitude plan. This map is extracted from the map presented in [20] and has spatial resolution of 12 arc second (which corresponds to 400m at this latitude). Below, we present the characteristics of the 2 scenarios and of the parameters of the 2 filters.

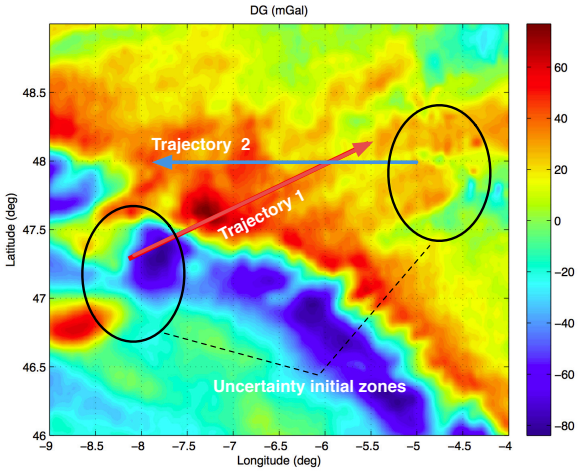

Fig. 8. Anomalies gravity map with the carrier's trajectories

Scenario parameters:

- Sampling period: $\Delta T = 10$ min
  Number of gravity measurements (12): 60
  Number of local minima: $m = 120$ (34)
  Resampling threshold: $N_{th} = \frac{1}{10} N$
  Importance functions (34): $\tilde{q}_k^1$ for the algorithm 1,

$\tilde{q}_k^2$ for the algorithm 2 with $\nu = 4$ (28)
Prior q_k: Gaussian for the algorithm 1, Student with $\nu = 4$ (28) for the algorithm 2. The mean and the covariance matrix of these priors are the empirical moments of the predicted particles (μ_k, P_k)

- Global Standard deviation of the gravity measurements (including map errors and gravity measurements errors): $\sigma_g = 3\,\text{mGal}$ (12)
  Carrier's dynamics noise = 0

- Number of particles: N=3000
  Initial uncertainty zone for the longitude and latitude: $\sigma = 0.1\,^\circ$ (which represents an area of 7x11 km^2 at latitude 48°)
  Initial uncertainty for the north and east velocities: $\sigma = 0.5\,\text{m/s}$
  Speed of the carrier: $\|V\| = 6\,\text{m/s}$

100 Monte Carlo trials have been performed. The root mean square error (RMSE), averaged over the 100 trials, is computed for the 4 components of the state vector: longitude, latitude, north and east velocities.

Scenario 1

The zone where the trajectory 1 starts presents severe ambiguities: many carrier trajectories starting from the uncertainty zone collect a similar anomaly measurements history (taking account the measurement noise) for the first 20 iterations (Fig. 9). At the beginning of this trajectory, there is a strong variation of the gravity anomaly (Fig. 10) which provides a great (local) information to the filter. But, in this context where the ambiguity is strong and where the initial uncertainty zone is large, we expect the filter to have a poor behavior. Indeed, we have observed 25 divergences for algorithm 1 and 11 divergences for algorithm 2. The latter shows a better robustness in this difficult quasi unobservable context. The improved filter can estimate temporarily a wrong trajectory but, due to the heavy tail of the IF, it can join the true one. We can see (Fig. 9) that some particles generated by the IF act as a kind of "trailblazer". The support (99.9 confidence ellipse) of the mesh is enlarged. The RMSE for the 4 components of the state vector is computed for the 2 algorithms only on the convergent trials (Fig. 11 & 12). During the first 30 iterations the anomaly gravity signal varies widely (Fig. 10) which leads to a fast convergence of the filters. Then the signal varies slowly and the estimation does not improve. We observe that the latitude is better estimated. This is due to the fact that the Eötvös effect, which depends on the latitude provides acceleration information (2) [1]. The Laplace-based resampling rate for algorithm 1 is about 21% and 15% for algorithm 2. For the 60 iterations, the computational cost is 13 s for the algorithm 1 and 9 s for the algorithm 2 on a 2.5 GHz Intel Core I5.

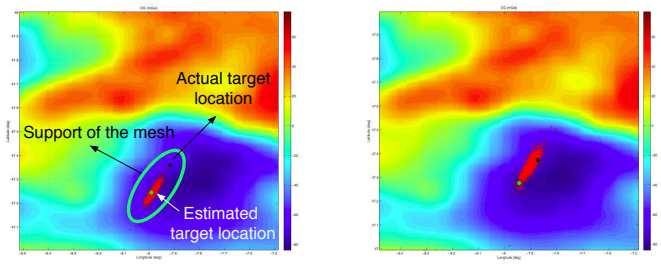

Fig. 9. illustration of the behavior of the heavy-tailed importance function (iterations 7 and 8)

Scenario 2

The trajectory 2 (Fig. 8) shows a slowly varying anomaly gravity signal (Fig. 10). However, the zone is less ambiguous that the one of the scenario 1. For the two algorithms we have observed 2% of divergences. The RMSE of these algorithms are comparable (Fig. 13 & 14) for the 4 components. The Laplace-based resampling (section **??**) rate for algorithm 1 is about 25% and 10% for algorithm 2. For the 60 iterations, the computational cost is 11 s for algorithm 1 and 6 s for algorithm 2.

The algorithm 2 offers a better robustness with a slightly better RMSE. Moreover, as the Laplace-redistributions are less frequent for this algorithm, the computational cost is reduced.

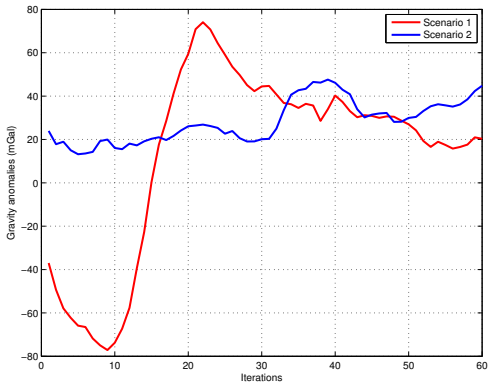

Fig. 10. Time history of the gravity anomaly for the 2 scenarios

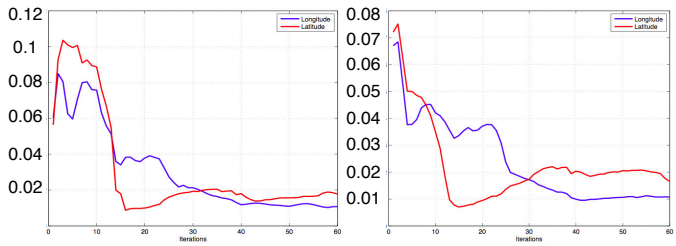

Fig. 11. Scenario 1. Position RMSE comparison of algorithm 1 (left figure) with algorithm 2 (right figure).

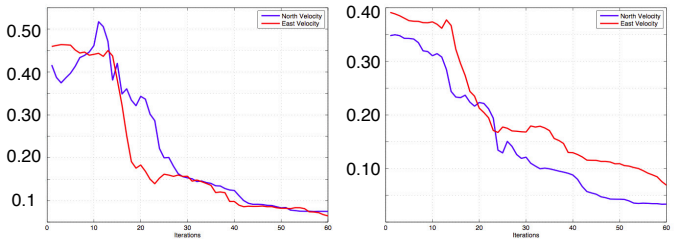

Fig. 12. Scenario 1. Velocity RMSE comparison of algorithm 1 (left figure) with algorithm 2 (right figure).

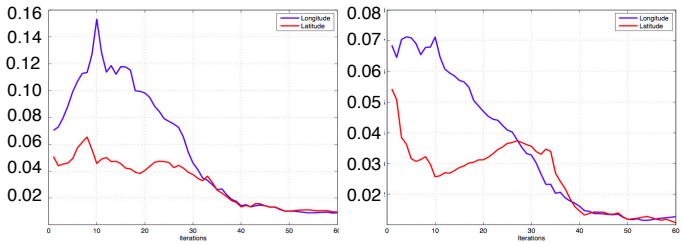

Fig. 13. Scenario 2. Position RMSE comparison of algorithm 1 (left figure) with algorithm 2 (right figure).

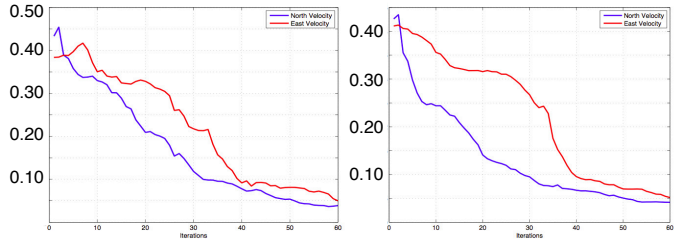

Fig. 14. Scenario 2. Velocity RMSE comparison of algorithm 1 (left figure) with algorithm 2 (right figure).

VI. Conclusion

We present the new version of the absolute gravimeter based on atom interferometry developed by ONERA. Based on it and on external measurements of the height of the carrier, we propose a method to map the gravity anomaly. The modified Laplace-based particle filter proposed for terrain-based navigation shows a better robustness in difficult contexts.

References

[1] Christian Musso, Alexandre Bresson, Yannick Bidel, Nassim Zahzam, Karim Dahia, Jean-Michel Allard, and Bernard Sacleux, "Absolute gravimeter for terrain-aided navigation," in *2017 20th International Conference on Information Fusion (Fusion)*. IEEE, 2017, pp. 1–7.

[2] Hugh F Rice and Vincent Benischek, "Submarine navigation applications of atom interferometry," in *Position, Location and Navigation Symposium, 2008 IEEE/ION*. IEEE, 2008, pp. 933–939.

[3] Yannick Bidel, Olivier Carraz, Renée Charrière, Malo Cadoret, Nassim Zahzam, and Alexandre Bresson, "Compact cold atom gravimeter for field applications," *Applied Physics Letters*, vol. 102, no. 14, pp. 144107, 2013.

[4] Ch J Bordé, "Atomic interferometry with internal state labelling," *Physics letters A*, vol. 140, no. 1-2, pp. 10–12, 1989.

[5] John F Clauser, "Ultra-high sensitivity accelerometers and gyroscopes using neutral atom matter-wave interferometry," *Physica B+ C*, vol. 151, no. 1-2, pp. 262–272, 1988.

[6] Pierre Gillot, Olivier Francis, Arnaud Landragin, F Pereira Dos Santos, and Sébastien Merlet, "Stability comparison of two absolute gravimeters: optical versus atomic interferometers," *Metrologia*, vol. 51, no. 5, pp. L15, 2014.

[7] Remi Geiger, Vincent Ménoret, Guillaume Stern, Nassim Zahzam, Patrick Cheinet, Baptiste Battelier, André Villing, Frédéric Moron, Michel Lours, Yannick Bidel, et al., "Detecting inertial effects with airborne matter-wave interferometry," *arXiv preprint arXiv:1109.5905*, 2011.

[8] Y Bidel, N Zahzam, C Blanchard, A Bonnin, M Cadoret, A Bresson, D Rouxel, and MF Lequentrec-Lalancette, "Absolute marine gravimetry with matter-wave interferometry," *Nat. Commun.*, vol. 9, pp. 627, 2018.

[9] Niclas Bergman, "Recursive bayesian estimation," *Department of Electrical Engineering, Linköping University, Linköping Studies in Science and Technology. Doctoral dissertation*, vol. 579, 1999.

[10] Achille Murangira and Christian Musso, "Proposal distribution for particle filtering applied to terrain navigation," in *Signal Processing Conference (EUSIPCO), 2013 Proceedings of the 21st European*. IEEE, 2013, pp. 1–5.

[11] M Sanjeev Arulampalam, Simon Maskell, Neil Gordon, and Tim Clapp, "A tutorial on particle filters for online nonlinear/non-gaussian bayesian tracking," *IEEE Transactions on signal processing*, vol. 50, no. 2, pp. 174–188, 2002.

[12] Paul Bui Quang, "Approximation particulaire et méthode de laplace pour le filtrage bayésien," 2013, Ph.D. thesis.

[13] Achille Murangira, "Nouvelles approches en filtrage particulaire. application au recalage de la navigation inertielle," 2014, Ph.D. thesis.

[14] Christian Musso, Frédéric Champagnat, and Olivier Rabaste, "Improvement of the laplace-based particle filter for track-before-detect," in *Information Fusion (Fusion), 2016 19th International Conference on*. IEEE, 2016.

[15] Neil J Gordon, David J Salmond, and Adrian FM Smith, "Novel approach to nonlinear/non-gaussian bayesian state estimation," in *IEE Proceedings F (Radar and Signal Processing)*. IET, 1993, vol. 140, pp. 107–113.

[16] Christian Musso, Paul Bui Quang, and Achille Murangira, "A laplace-based particle filter for track-before-detect," in *Information Fusion (Fusion), 2015 18th International Conference on*. IEEE, 2015, pp. 1657–1663.

[17] Paul Bui Quang, Christian Musso, and François Le Gland, "Multi-dimensional laplace formulas for nonlinear bayesian estimation," in *Signal Processing Conference (EUSIPCO), 2012 Proceedings of the 20th European*. IEEE, 2012, pp. 1890–1894.

[18] Pierre Del Moral and Feynman-Kac Formulae, "Genealogical and interacting particle systems with applications, probability and its applications," 2004.

[19] Augustine Kong, Jun S Liu, and Wing Hung Wong, "Sequential imputations and bayesian missing data problems," *Journal of the American statistical association*, vol. 89, no. 425, pp. 278–288, 1994.

[20] David T Sandwell, R Dietmar Müller, Walter HF Smith, Emmanuel Garcia, and Richard Francis, "New global marine gravity model from cryosat-2 and jason-1 reveals buried tectonic structure," *Science*, vol. 346, no. 6205, pp. 65–67, 2014.